Two-platinum-atom complex defects in silicon - an electron paramagnetic resonance study

1999 J. Phys.: Condens. Matter 11 7615

(http://iopscience.iop.org/0953-8984/11/39/316)

J. Phys.: Condens. Matter **11** (1999) 7615–7625. Printed in the UK PII: S0953-8984(99)04651-2

Two-platinum-atom complex defects in silicon—an electron paramagnetic resonance study

U Juda and M Höhne
Institut für Kristallzüchtung Berlin–Adlershof, Rudower Chaussee 6, D-12489 Berlin, Germany

Received 28 May 1999

Abstract. Previously, two complex orthorhombic defects containing two platinum atoms were detected in silicon by means of electron paramagnetic resonance. In this paper other two-Pt-atom defects are investigated, an orthorhombic one and a monoclinic one. The spin Hamiltonians of these defects are given. Features of the monoclinic defect suggest a pair of Pt atoms positioned in a divacancy.

Additional information about the structures of the different defects emerges from the conditions of sample preparation. Arguments are considered which suggest that the orthorhombic defect is a different charge state of one of the known two-Pt-atom defects. The monoclinic defect is formed only in samples which are assumed to be supersaturated with self-interstitials.

1. Introduction

The properties of silicon are substantially modified by doping with platinum. The isolated platinum atom at a substitutional lattice site (Pt_s) acts as a donor or an acceptor according to the properties of the starting material [1, 2]. The electronic structure of this defect is well known from electron paramagnetic resonance (EPR) investigation of its negative charge state Pt_s^- [3–6]. The limiting of the carrier lifetime in silicon by doping with platinum was attributed for decades to Pt_s, but has more recently been attributed to complex platinum-related defects [7–9]. The electrical levels of complex platinum-related defects differ substantially from the levels of Pt_s [10]. This is a reason for investigating complex Pt-related defects.

Complex defects containing only one Pt atom (called 1-Pt defects) are pairs of Pt with manganese [3] or iron [11], or complexes with two hydrogen atoms [12,13], one and two lithium atoms [14], or an unknown number of carbon atoms [15]. Two three-Pt-atom defects were detected by means of EPR. One is hydrogen related [13]; the other one is carbon related [15]. The biggest Pt clusters contain six Pt atoms. We know two six-Pt-atom clusters of symmetry D_{3d} and one type of symmetry C_{2h} [16, 17].

The subject of this paper is the comparison of new two-Pt-atom complexes with known ones. The first two-Pt-atom defect (we will call it 2-Pt(1)) detected by means of EPR was attributed to a Pt–Pt pair without additional components of the complex [18]. The detection of a second two-Pt-atom complex (called 2-Pt(2)) made the identification questionable [19]. The symmetries of both complexes are orthorhombic, and in both complexes the Pt atoms are geometrically equivalent. However, the parameters of the spin Hamiltonian differ substantially. Therefore, at least one of these two-Pt-atom defects was expected to contain another defect besides the two Pt atoms. In this paper another orthorhombic two-Pt-atom defect and a monoclinic one will be characterized by their spin Hamiltonians. The preparation conditions will be compared.

0953-8984/99/397615+11$30.00

2. Experiment

2.1. Sample preparation

The starting materials were floating-zone-Si (FZ-Si) and Czochralski-Si (Cz-Si) of both n type and p type. The concentrations of donors and acceptors, respectively, were typically in the range between 1×10^{15} cm^{-3} and 1×10^{17} cm^{-3} with a negligible degree of compensation.

The samples, of $3 \times 3 \times 10$ mm^3 size, were doped with Pt by covering the surface with a metallic layer and subsequent annealing at 1200–1300 °C in an Ar atmosphere or in vacuum. The time of annealing ranged from several hours to three days. In order to prevent contamination during this procedure, the samples were kept in a double-walled quartz tube with a chlorine-containing gas flow in the outer tube. The efficiency of this system was confirmed by controlling the contamination with the fast-diffusing omnipresent iron from the stove. When the system works, the concentration of Pt–Fe pairs detected by means of EPR is below the level of detection [11].

Usually the layer of metallic Pt was deposited on the surface from a spin-on dopant manufactured by Filmtronics Incorporated, Butler, PA. For comparison, several different samples were covered with Pt by sputtering in order to exclude the possibility of an influence of the commercial solution on the phenomena to be described below. The results obtained by the two methods were the same.

The formation of certain complexes depends on the presence of additional defects which are assumed to be self-interstitials. In such samples various typical phenomena related to specific defects were detected [10, 20]. Therefore, two types of sample were prepared and compared.

(i) The first type are obtained when, after the doping procedure described above has been carried out, the sample is quenched to room temperature. Before the EPR measurement was made or further thermal treatment at temperatures between 450 and 540 °C was carried out, a surface layer 100 μm thick was carefully removed. We will refer to such samples in the following as 'quenched after annealing with a covered surface'. Previous investigation showed that such samples exhibit a high degree of supersaturation with self-interstitials [21].

(ii) The second type of samples were obtained by annealing samples quenched after annealing with a covered surface once more for one day at 1200–1300 °C in vacuum, now without a metallic or reaction layer on the surface. We will refer to such samples as 'quenched after annealing with an uncovered surface'. It is suggested that as a result of this treatment the supersaturation with self-interstitials has been removed [10, 20]. Some of the complex defects to be discussed in this paper are not formed in these samples.

2.2. EPR measurement

The EPR measurements were done on a Bruker spectrometer ESP 300 E operating at a microwave frequency of $\nu = 9.43$ GHz. A continuous-flow cryostat from Oxford Instruments was applied. It was slightly modified in order to shield the sample from thermal radiation emitted by the walls of the EPR cavity [10]. In photo-EPR experiments the sample inside the quartz walls of the cryostat was illuminated through a quartz lens and the grid of the Bruker universal rectangular resonator.

3. Results

3.1. Orthorhombic two-Pt-atom complexes

Defects containing two platinum atoms were detected by EPR investigation. The Zeeman part of the spin Hamiltonian is

$$\mathcal{H}_{Ze} = \mu_B(B_x g_{xx} S_x + B_y g_{yy} S_y + B_z g_{zz} S_z + B_y g_{yz} S_z + B_z g_{zy} S_y) \tag{1}$$

with axes x and y in $\langle 110\rangle$ directions and z in a $\langle 100\rangle$ direction and with $g_{yz} = g_{zy} = 0$ in the case of orthorhombic symmetry. In this case the axes x, y, z coincide with the defect principal axes X, Y, Z. The components of the applied magnetic field $\boldsymbol{B}$ and the spin of the electron are B_k and S_k $(k = x, y, z)$; μ_B is the Bohr magneton. For all of the complex defects investigated in this paper, the effective electron spin is $S = 1/2$.

Instead of a single resonance line caused by a Zeeman transition, a group of lines is detected in the EPR experiment due to the hyperfine interaction with the ^{195}Pt nucleus which has a nuclear spin $I = 1/2$ with a natural abundance of 33.8%. In the following, such groups are called hyperfine groups. The interaction with one Pt nucleus causes a splitting into three lines with relative intensities near to the ratio 1:4:1. Because of the interaction with a second Pt nucleus each of these three lines is split according to the same ratio. If the line distances of the two splittings are equal, i.e. when the atoms are equivalent, the resulting hyperfine group consists of five lines with relative intensities near to 1:8:18:8:1.

Each of the Pt atoms realizes a local symmetry of point group C_{1h}. The spin Hamiltonian of the hyperfine interaction with the two Pt nuclei labelled $j = 1, 2$ is

$$\mathcal{H}_{hf} = \sum_{j=1}^{2} (S_{\xi^{(j)}} A_\xi I_{\xi^{(j)}} + S_{\eta^{(j)}} A_\eta I_{\eta^{(j)}} + S_{\zeta^{(j)}} A_\zeta I_{\zeta^{(j)}}). \tag{2}$$

The arrangement of the principal axes $\xi^{(j)}$, $\eta^{(j)}$, and $\zeta^{(j)}$ is shown in figure 1(a). The axes $\xi^{(1)}$ and $\xi^{(2)}$ coincide with the x-axis. The systems of coordinates $\eta^{(1)}, \zeta^{(1)}$ and $\eta^{(2)}, \zeta^{(2)}$ are created by rotating the system y, z about the x-axis through $\rho^{(1)}$ and $\rho^{(2)} = -\rho^{(1)}$, respectively. The fact that the principal values A_ξ, A_η, A_ζ are not labelled $j = 1, 2$ corresponds to the geometrical equivalence of the two Pt nuclei. In figure 1 the yz-plane is represented.

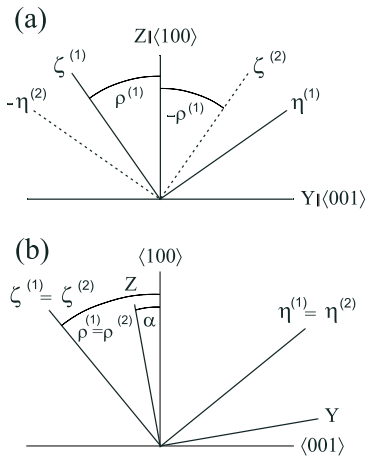

Figure 1. Principal axes in the mirror planes of two-Pt-atom defects: Y, Z for the g-tensor, $\eta^{(j)}$ and $\zeta^{(j)}$ for the hyperfine tensors; (a) orthorhombic defects; (b) monoclinic defects.

The parameters of the spin Hamiltonians $\mathcal{H}_{Ze}$ and $\mathcal{H}_{hf}$ are determined from the angular dependence of the spectra according to the procedure described previously [19].

For the two-Pt-atom defects the parameters of the spin Hamiltonian are given in table 1. The defects 2-Pt(1) to 2-Pt(3) are of orthorhombic symmetry. This is indicated by the value of the angle $\alpha = 0$. This angle will be defined in section 3.2, it characterizes the deviation of the defect system X, Y, Z from the crystal axes x, y, z.

Table 1. EPR parameters of two-Pt-atom defects.

Defect	g_X	g_Y	g_Z	$\lvert A_\xi \rvert$[a]	$\lvert A_\eta \rvert$[a]	$\lvert A_\zeta \rvert$[a]	α	$\rho^{(1)}$	$\rho^{(2)}$
2-Pt(1)[b]	2.1869	1.5181	1.6317	52	69	85	0	55	−55
2-Pt(2)[c]	2.1107	2.1631	2.1755	30	43	9	0	61	−61
2-Pt(3)[d]	2.1113[e]	2.3144[e]	2.0968[e]	17 ± 3	19 ± 3	41 ± 3	0	53 ± 5	-53 ∓ 5
2-Pt(4)[d]	1.5373[f]	1.8448[f]	1.8135[f]	132 ± 3	121 ± 3	158 ± 3	9.5 ± 1	48 ± 1	48 ± 1

[a] In units of 10^{-4} cm^{-1}.
[b] Reference [18].
[c] Reference [19].
[d] This paper.
[e] ± 0.0003.
[f] ± 0.0005.

Like the previously investigated defects 2-Pt(1) and 2-Pt(2), the defect 2-Pt(3) also does not exhibit a hyperfine structure besides that caused by the Pt nuclei. However, constituents with nonzero nuclear spin may exist if the hyperfine interaction is too small to be resolved in the EPR experiment. We detected 2-Pt(1) defects only in silicon samples with a high concentration of acceptors. The possibility of a Pt–Pt pair bound to a boron atom could be excluded by investigating samples doped with a similar concentration of the acceptor gallium instead of boron. The parameters of the spin Hamiltonian were the same for the 2-Pt(1) defects in the two types of material.

The 2-Pt(2) defects were detected only in n-type silicon in the dark. The EPR spectra were completely annihilated by illuminating the sample with band-gap light. The 2-Pt(3) defects were detected in p-type silicon in the dark and in n-type silicon only under illumination. The two types of defect follow the same rules of formation and destruction. They are present in samples quenched after annealing with a covered surface or with an uncovered one, respectively. Their concentrations increase during annealing at 200 °C. They are destroyed by annealing at 350 °C. These facts give rise to the supposition that the two types of defect are different charge states of the same defect. The optimum temperature for the EPR detection of both the 2-Pt(2) and 2-Pt(3) defects was 20 K for our equipment, whereas the 2-Pt(1) defects were detected at 8 K together with Pt_S. All three orthorhombic two-Pt-atom defects were found in samples quenched after annealing at 1200 °C, irrespective of whether they were annealed with a covered surface or with an uncovered one.

3.2. A monoclinic two-Pt-atom complex

In this section we report on the EPR investigation of a monoclinic defect containing two Pt atoms. The formation of this defect is restricted to samples quenched after annealing with a covered surface (see section 2.1).

The Zeeman part of the spin Hamiltonian is given by (1) again with axes x and y in $\langle 110 \rangle$ directions and z in a $\langle 100 \rangle$ direction. The mirror plane (see figure 1(b)) is perpendicular to the x-axis. As in section 3.1 for the hyperfine matrix, here a symmetric g-matrix is assumed, i.e. $g_{zy} = g_{yz}$. In this sense the term g-tensor is used. The principal axes X, Y, Z for the

g-tensor are obtained in the present case from the system x, y, z by rotating about the x-axis through an angle α (see figure 1(b)). The magnetic field $\boldsymbol{B}$ is in such a direction that it has direction cosines $\lambda_X, \lambda_Y, \lambda_Z$ with respect to X, Y, Z. The Zeeman part of the spin Hamiltonian is now

$$\mathcal{H}_{Ze}^{(m)} = \mu_B(B_X g_X S_X + B_Y g_Y S_Y + B_Z g_Z S_Z). \tag{3}$$

In an experiment where the sample is rotated about a ⟨110⟩ axis, the various orientations of the monoclinic defect in the cubic lattice are characterized by seven sets of $\lambda_X, \lambda_Y, \lambda_Z$. The seven corresponding g-values

$$g = \sqrt{\lambda_X{}^2 g_X{}^2 + \lambda_Y{}^2 g_Y{}^2 + \lambda_Z{}^2 g_Z{}^2} \tag{4}$$

determine the field values $B = h\nu/(g\mu_B)$ of the central lines in the hyperfine groups (see section 3.1). Here h is Planck's constant. The angular dependences of these central-line positions are given in figure 2. We define an angle of rotation which is zero for $\boldsymbol{B} \parallel \langle 100 \rangle$. The bold lines represent a dense sequence of experimental points. Thin parts of the lines were calculated and indicate that the 2-Pt(4) spectrum is covered by the Pt_s^- spectrum. The principal values g_X, g_Y, and g_Z determined from the angular dependence are included in table 1. The angle $\alpha = 9.5$ was determined within small margins of error.

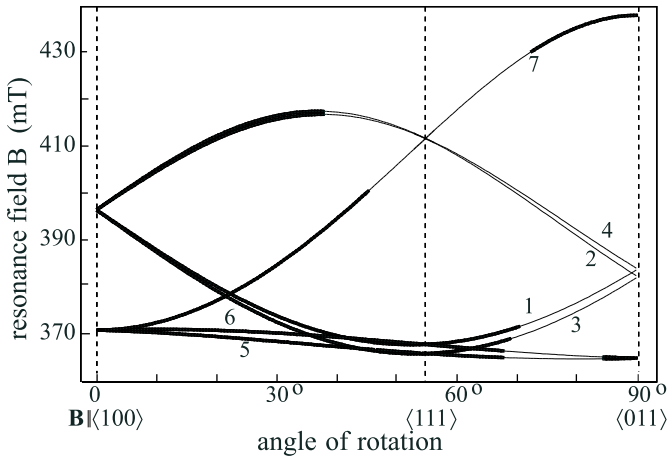

Figure 2. Angular dependences of the central-line positions for rotation of the magnetic field in a {110} plane. Seven different orientations of monoclinic defects occur.

In figure 3 the spectrum was recorded with a sample at 20 K for a direction of the magnetic field $\boldsymbol{B}$ nearly parallel to a ⟨100⟩ direction. The bars above the spectrum indicate the hyperfine splitting due to two equivalent Pt nuclei. When the condition $\boldsymbol{B} \parallel \langle 100 \rangle$ is exactly fulfilled, the two groups near 396 mT (labelled 2, 4 and 1, 3, respectively, in figure 2) coincide.

Hyperfine groups resulting from the Zeeman transitions (labelled 1, 3, 5, and 6 in figure 2) are given for the angles of rotation 54.7°, i.e. $\boldsymbol{B} \parallel \langle 111 \rangle$, in figure 4(a), for 60° in figure 4(b), and for 65° in figure 4(c). Arrows point to the central lines of the hyperfine groups. Even in the case of exact orientation of the sample, these groups do not coincide for $\boldsymbol{B} \parallel \langle 111 \rangle$ which would happen for orthorhombic symmetry of the paramagnetic defects. This proof of lower symmetry is confirmed by the fact that groups 1 and 6 on the one hand and groups 3 and 5 on the other hand exhibit substantially different hyperfine splittings in spite of having very similar g-values. These splittings are demonstrated as bars above the spectrum in figure 4(a).

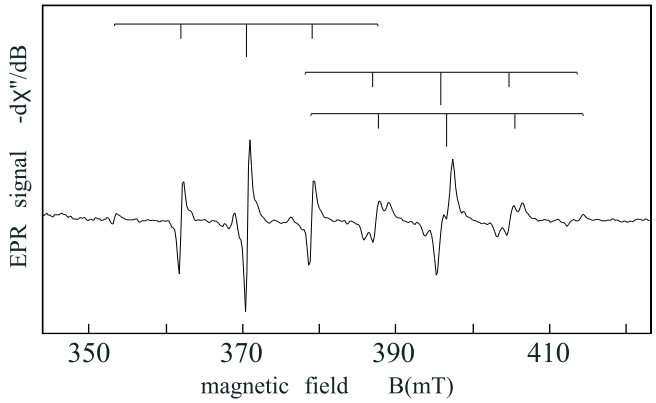

Figure 3. The EPR spectrum of 2-Pt(4) defects at 8 K for $\boldsymbol{B} \parallel \langle 100 \rangle$.

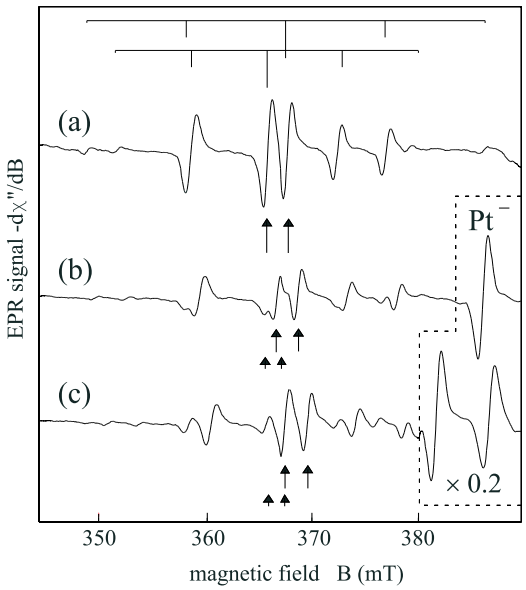

Figure 4. EPR spectral groups 1, 3, 5, and 6 (see figure 2) measured at 8 K for three angles of rotation: (a) 54.7° ($\boldsymbol{B} \parallel \langle 111 \rangle$), (b) 60°, (c) 65°. For (a), bars indicate the hyperfine splittings.

The hyperfine interaction with the two Pt nuclei represented by the spin Hamiltonian of (2) is treated as a perturbation that is small compared to the Zeeman interaction. We define $\Delta^{(j)} = \rho^{(j)} - \alpha$ and δ and θ by the equations

$$\sin\delta = \lambda_X g_X / \sqrt{(\lambda_X g_X)^2 + (\lambda_Y g_Y)^2} \tag{5}$$

and

$$\cos\theta = \lambda_Z g_Z / g. \tag{6}$$

The line positions are given by

$$B = \frac{h\nu}{g\mu_B} - \frac{1}{g\mu_B}(K^{(1)}m^{(1)} + K^{(2)}m^{(2)}) \tag{7}$$

with

$$K^{(j)} = \left([A_\xi \sin\theta \sin\delta]^2 + [A_\eta(\cos\delta \sin\theta \cos\Delta^{(j)} - \cos\theta \sin\Delta^{(j)})]^2 + [A_\zeta(\cos\delta \sin\theta \sin\Delta^{(j)} + \cos\theta \cos\Delta^{(j)})]^2\right)^{1/2}. \quad (8)$$

$K^{(j)}$ and $m^{(j)}$ are the hyperfine splitting parameters and the nuclear quantum numbers of the ^{195}Pt nuclei ($j = 1, 2$).

The 2-Pt(4) defect differs from the orthorhombic ones by having the striking property that the two Pt nuclei are magnetically equivalent ($K^{(1)} = K^{(2)}$) for all angles of rotation and all groups of defect orientations. This means that not only are the components A_ξ, A_η, and A_ζ equal for the two Pt nuclei, but so also are the principal axes of the hyperfine interaction tensor:

$$\xi^{(1)} = \xi^{(2)} \qquad \eta^{(1)} = \eta^{(2)} \qquad \zeta^{(1)} = \zeta^{(2)}.$$

This situation is illustrated in figure 1(b). Of course, $\rho^{(1)} = \rho^{(2)}$ is also true.

For the six hyperfine groups in the measurement of the angular dependence the experimental value of $K^{(1)} = K^{(2)}$ could be determined easily. These groups are indicated in figure 5 by circles. The six values were used to fit the four parameters A_ξ, A_η, A_ζ, and $\rho^{(1)} = \rho^{(2)}$ and to estimate the margins of error. The parameters are given in table 1. They were used to calculate the curves in figure 5.

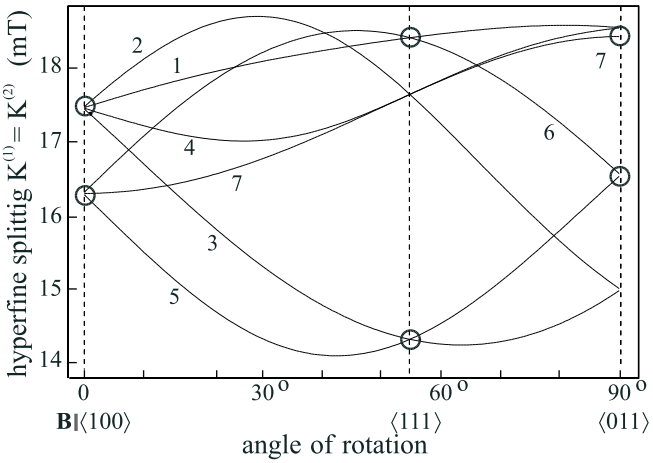

Figure 5. Angular dependences of the hyperfine splittings $K^{(j)} \times (hc)/(g\mu_B)$ for rotation of the magnetic field in a {110} plane. The defect orientations are labelled as in figure 2.

Figure 2 shows the resonance fields instead of the g-values and figure 5 shows the field splittings $K^{(j)} \times (hc)/(g\mu_B)$ in order to facilitate the comparison of figure 2 to figure 5. Here c is the velocity of light.

The seven groups resulting from different defect orientations are labelled in the same way as in figure 2. The calculated values are in agreement with the experimental results also for the other positions in the angular dependence (see e.g. figures 4(a) and 4(b)).

3.3. Discussion

The simplest model compatible with the overall symmetry of the orthorhombic defects and the fact of two geometrically equivalent Pt atoms is given in figure 6 which shows the mirror plane of the defect. The symmetry group is C_{2v}. The Pt atoms are at substitutional sites in a

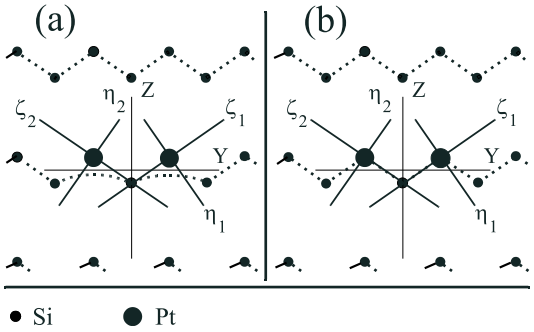

Figure 6. Orthorhombic two-Pt-atom defects: (a) the model related to the vacancy model [6]; (b) the model related to the dihedral model [4]. Bonds are indicated by broken lines.

next-nearest-neighbour (n.n.n.) arrangement. One can imagine that the Pt atoms have closed shells with the electron spin density mainly in the reconstructed bonds of the Si neighbours (see figure 6(a)) in the sense of the vacancy model of Pt_s^- [6]. One cannot exclude the possibility that in the case of a two-Pt-atom defect a predominant bonding of each Pt atom with two Si neighbours exists (see figure 6(b)) in the sense of a dihedral model of Pt_s^- [4]. In any case, table 1 and figure 1(a) show that each of the Pt atoms has a principal axis of the hyperfine interaction tensor nearly in a $\langle 111 \rangle$ direction towards the nearest neighbour common to both Pt atoms.

As noticed in section 1, at most one of the orthorhombic two-Pt-atom defects can be identified with the true Pt–Pt pair—that is, without additional constituents of the complex defect. For comparison we quote data for Pt_s^-: $g_x = 1.3865$, $g_y = 1.4265$, $g_z = 2.0789$, $A_x = 148 \times 10^{-4}$ cm^{-1}, $A_y = 186 \times 10^{-4}$ cm^{-1}, $A_z = 127 \times 10^{-4}$ cm^{-1} [5]. When hyperfine interaction parameters of single defects and pairs are compared, one must keep in mind that in the latter case the spin density is distributed over two nuclei [25].

As mentioned at the end of section 3.1, there are experimental facts which suggest that the two defects 2-Pt(2) and 2-Pt(3) are different charge states of the same defect. This suggestion is supported by the fact that in n-type silicon the disappearance of the 2-Pt(2) defects under illumination is accompanied by the appearance of 2-Pt(3) defects. Arguments against this suggestion derive first from the fact that the concentration of 2-Pt(3) defects produced under illumination does not equal the concentration of the disappearing 2-Pt(2) defects. Second, in p-type silicon the 2-Pt(2) defects were not detected when the 2-Pt(3) defects were annihilated by illumination with band-gap light. However, both contradictions can be resolved by the assumption of a third charge state between the two paramagnetic ones. Then, under illumination the upper charge state would be occupied only partly or not at all. This assumption agrees well with the fact that both the 2-Pt(2) and 2-Pt(3) spectra are described by spin $S = 1/2$.

Unfortunately, a proof of an additional element in the 2-Pt(2, 3) defects is not obtained from the hyperfine structure. Therefore, only hints from the preparation are available. The most prominent impurities can be excluded from consideration. This is true for oxygen because there is no difference between Cz- and FZ-Si. The concentration of the defects was not enhanced in materials additionally doped with iron, chromium, hydrogen, and carbon.

A strong argument against the incorporation of acceptor atoms in these defects arises from the fact that the g-parameters are the same in Si doped with gallium or indium instead of boron.

In our samples other impurities should not be present in a concentration necessary for

the production of 1×10^{15} cm^{-3} defects, which is nearly the concentration of the 2-Pt(2, 3) defects.

Therefore, the most probable speculation concerning a model of the 2-Pt(2, 3) defects suggests either the participation of an intrinsic defect or the possibility that these defects represent the true orthorhombic Pt pair. The latter interpretation would imply that the 2-Pt(1) defect contains an additional element.

Models for the 2-Pt(4) defect are considered with the aid of figure 7. The symmetry group of the models is C_{2h}. With a magnetic field rotated in the plane of the drawing, the defects sketched in the left-hand parts of figure 7 represent defect orientations labelled 5 in figure 2 and figure 5. The sketches in the right-hand parts correspond to the groups labelled 6 in those figures.

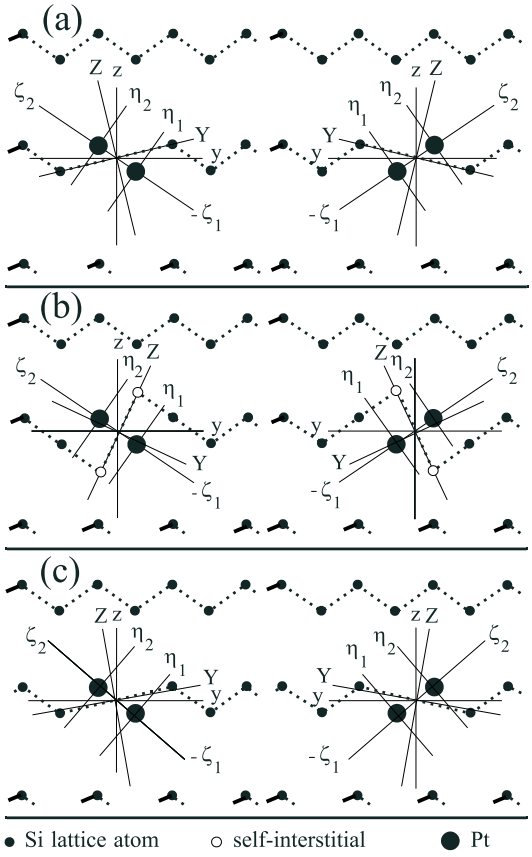

Figure 7. Monoclinic 2-Pt defects: (a) the model related to the divacancy [22–24]; (b) the model with self-interstitials at tetrahedral interstitial sites; (c) the principal axes of *g*- and hyperfine interaction tensors determined from the experiment. Bonds are indicated by broken lines.

The fact that for $\boldsymbol{B} \parallel \langle 111 \rangle$ the hyperfine splittings of the groups 5 and 6 are near to their maximum and minimum values, respectively, strongly suggests a nearest-neighbour arrangement of the two Pt atoms. This is assumed in all parts of figure 7 where the Pt atoms are represented as big full circles.

Keeping in mind the vacancy model for the isolated Pt_s defect, we took into account the EPR investigation of the divacancy [22–24]. This leads to the model demonstrated in

figure 7(a). Two Pt atoms with closed d shells are positioned in the divacancy. As inferred from the previous results on the divacancy, the paramagnetic state of the defect is mainly localized in the extended orbital between the two Si atoms neighbouring the divacancy in the plane of the drawing. Taking the straight line between these lattice sites as a principal axis of the g-tensor, one would roughly expect $Y \parallel \langle 133 \rangle$ corresponding to an angle of $\alpha = 13^\circ$ between Y and the crystal lattice direction $y \parallel \langle 011 \rangle$ or between Z and $z \parallel \langle 100 \rangle$. Considering figure 1(b), one obtains

$$\Delta^{(2)} = \Delta^{(1)} = \rho^{(1)} - \alpha = 55^\circ - 13^\circ = 42^\circ.$$

This difference will be compared with a value emerging from the experiment according to equations (7) and (8).

Another model is offered in figure 7(b). We know that the formation of 2-Pt(4) defects occurs only after a treatment which is assumed to create a supersaturation of the sample with self-interstitials. Therefore, one might include two additional silicon atoms at tetrahedral interstitial sites in the extended orbital. The self-interstitials are represented as empty circles. Roughly approaching a principal axis of the g-tensor along the straight line between these sites, one obtains $\alpha = -25^\circ$ and $\Delta^{(1)} = \Delta^{(2)} = 80^\circ$.

In figure 7(c), the principal axes of the g-tensor and the hyperfine tensors are directed according to the values in table 1: $\alpha = 9.5^\circ$ and

$$\Delta^{(1)} = \Delta^{(2)} = \rho^{(1)} - \alpha = 38.5^\circ.$$

These values result from fitting the experimental data (see section 3.2). They are near to those from the model considered in figure 7(a). Obviously, this model is preferred to that of figure 7(b). We notice that the hyperfine interaction of the 2-Pt(4) defects is stronger than that of all other two-Pt-atom defects.

In our opinion, the existence of both an orthorhombic true two-Pt-atom pair and a monoclinic one without additional elements is possible. One should keep in mind that after quenching the defects are not in an equilibrium state. As known from the preparation procedure, the conditions are different at the elevated temperature of defect formation. In the case of the 2-Pt(4) defect, the presence of other elements, probably self-interstitials, may stabilize the nearest-neighbour arrangement. During the cooling down to room temperature, the more mobile additional defects may dissociate and be trapped elsewhere.

4. Conclusions

In silicon doped with Pt, various electrically active complex defects are formed besides the isolated substitutional defect. The detection depends on the concentrations of shallow donors or acceptors, and on the thermal history of the samples. An orthorhombic two-Pt-atom defect was detected which is possibly a different charge state of a previously detected two-Pt-atom defect. The EPR investigation does not give a hint as to the additional constituents of the complexes.

The EPR spectrum of a monoclinic two-Pt-atom defect suggests a model with two Pt atoms at nearest-neighbour sites in a divacancy. This means the existence of a true monoclinic Pt–Pt pair besides a possibly existing orthorhombic one.

Some complex defects are formed only in samples quenched after annealing with a surface covered by metallic Pt. The paramagnetic six-Pt-atom clusters (see section 1) and the monoclinic two-Pt-atom defect belong to this group of defects. Although samples treated in this way are assumed to be supersaturated with self-interstitials, the model of the monoclinic two-Pt-atom defect does not contain self-interstitials. One might suggest that close packing of Pt

atoms in the monoclinic two-Pt-atom defect and the formation of the big six-Pt-atom clusters are enabled by a surplus of self-interstitials. This surplus would enlarge the concentration of the mobile Pt atoms at interstitial sites compared with that of substitutional Pt in the temperature range of complexing.

References

[1] Lemke H 1984 *Phys. Status Solidi* a **86** K39–42
[2] Zimmermann H and Ryssel H 1990 *Appl. Phys. Lett.* **58** 499–501
[3] Ludwig G W and Woodbury H H 1962 *Solid State Physics* vol 13 (New York: Academic) pp 223–304
[4] Ammerlaan C A J and van Oosten A B 1989 *Phys. Scr.* T **25** 342–7
[5] Anderson F G, Milligan R F and Watkins G D 1992 *Phys. Rev.* B **45** 3279–86
[6] Anderson F G, Ham F S and Watkins G D 1992 *Phys. Rev.* B **45** 3287–303
[7] Stöffler W and Weber J 1986 *Phys. Rev.* B **33** 8892–5
[8] Kwon Y K, Ishikawa T and Kuwano H 1987 *J. Appl. Phys.* **61** 1055–8
[9] Sachse J-U, Sveinbjörnsson E Ö, Jost W and Weber J 1997 *Appl. Phys. Lett.* **70** 1584–6
[10] Juda U, Scheerer O, Höhne M, Riemann H, Schilling H-J, Donecker J and Gerhardt A 1996 *J. Appl. Phys.* **80** 3435–44
[11] van Oosten A B, Son N T, Vlasenko L S and Ammerlaan C A J 1989 *Mater. Sci. Forum* **38–41** 355–60
[12] Williams P M, Watkins G D, Uftring S and Stavola M 1993 *Phys. Rev. Lett.* **70** 3816–19
[13] Höhne M, Juda U, Martynov Y V, Gregorgiewicz T, Ammerlaan C A J and Vlasenko L S 1994 *Phys. Rev.* B **49** 13 423–9
[14] Alteheld P, Greulich-Weber S, Spaeth J-M, Weihrich H, Overhof H and Höhne M 1995 *Phys. Rev.* **52** 4998–5006
[15] Scheerer O, Höhne M and Juda U 1997 *J. Appl. Phys.* **82** 3456–61
[16] Höhne M and Juda U 1992 *J. Appl. Phys.* **72** 3095–101
[17] Höhne M and Juda U 1995 *Mater. Sci. Technol.* **11** 680–3
[18] von Bardeleben H J, Stíevenard D, Brousseau M and Barrau J 1988 *Phys. Rev.* B **38** 6308–11
[19] Höhne M 1992 *Phys. Rev.* B **45** 5883–6
[20] Scheerer O, Juda U and Höhne M 1998 *Phys. Rev.* B **57** 9657–62
[21] Baumann F H and Schröter W 1991 *Phys. Rev.* B **43** 6510–19
[22] Watkins G D and Corbett J W 1965 *Phys. Rev.* **138** A543–55
[23] Corbett J W and Watkins G D 1965 *Phys. Rev.* **138** A555–60
[24] de Wit G, Sieverts E G and Ammerlaan C A J 1976 *Phys. Rev.* B **14** 3494–503
[25] Bencini A and Gatteschi D 1990 *EPR of Exchange Coupled Systems* (Berlin: Springer) p 42